DOI: 10.15244/pjoes/209222

ONLINE PUBLICATION DATE: 2025-12-01

Original Research

# Analysis of Groundwater Dynamic Change and Influencing Factors in Rizhao Coastal Plain Area

Yuan Jie<sup>1</sup>, Zhao Xiaoxin<sup>1</sup>, Yao Dongxu<sup>2</sup>, Wei Tongzheng<sup>10\*</sup>, Lv Youcheng<sup>1,3,4,5</sup>

<sup>1</sup>No. 8 Institute of Geology and Mineral Resources Exploration of Shandong Province, Rizhao, Shandong, 276826, China <sup>2</sup>Institute of Geographic Sciences and Natural Resources Research, Chinese Academy of Sciences, Beijing, 100010, China

<sup>3</sup>Key Laboratory of Nonferrous Metal Ore Exploration and Resource Evaluation of Shandong Provincial Bureau of Geology and Mineral Resources, Rizhao, Shandong, 276826, China

<sup>4</sup>Rizhao Big Data Research Institute of Geology and Geographic Information, Rizhao, Shandong, 276826, China <sup>5</sup>Rizhao Key Laboratory of Land Quality Evaluation and Pollution Remediation, Rizhao, Shandong, 276826, China

Received: 24 June 2025 Accepted: 10 August 2025

## Abstract

Groundwater dynamics in the Rizhao Coastal Plain, primarily Quaternary porous phreatic aquifers, exhibit complex spatiotemporal variability driven by natural and anthropogenic factors. Using 2018-2020 monitoring data from 20 wells, the dynamic variation of groundwater in the Rizhao Coastal Plain was studied by applying empirical orthogonal function (EOF) decomposition, spatial analysis, and correlation analysis. EOF decomposition revealed distinct seasonal patterns: groundwater level fluctuations demonstrated lower interquartile ranges in summer-autumn than in winter-spring (p<0.05). Spatial analysis identified four principal components explaining 83.2% of the total variance (PC1 = 36.7%, PC2 = 24.2%, PC3 = 13.4%, PC4 = 8.9%). Precipitation accounted for 45.6% of level variations, with anthropogenic activities (e.g., groundwater extraction) contributing 54.4%. By 2020, intensive extraction displaced the piezometric centroid southwestward, forming a new depression cone. To maintain aquifer equilibrium and prevent seawater intrusion, integrated management strategies are imperative: 1) Optimizing socio-economic spatial planning to reduce extraction pressure; 2) Implementing dynamic water allocation systems; 3) Establishing cross-sectoral governance frameworks for coordinated aquifer protection. This study provides a scientific basis for sustainable groundwater utilization in coastal plains undergoing rapid development.

Keywords: Rizhao, groundwater regime, Futuan River, rainfall, EOF analysis, strand plain

\_\_

<sup>\*</sup>e-mail: weitongzheng2024@163.com °ORCID iD: 0009-0008-0733-1714

### Introduction

Groundwater in coastal plain areas is an important freshwater resource [1, 2]. Globally, coastal plains are also densely populated regions, and groundwater in these areas plays a crucial role in socioeconomic development, production, and daily life [3, 4]. Research on groundwater dynamics is essential for the management and sustainable utilization of groundwater resources [5, 6]. China has an extensive coastline, with coastal plains primarily located along the eastern seaboard. The groundwater resources in these coastal plains are vital natural resources indispensable for economic and social development [7, 8].

Extensive research on groundwater dynamics in coastal plains has been conducted worldwide over the past decades. These studies have consistently demonstrated significant spatial variability groundwater behavior. Subba et al. used Geochemical Ratios (GR), Pollution Index of Groundwater (PIG), and Unmixing Model (UM) to help determine the changes in groundwater chemistry and groundwater quality in the rural areas of Telangana, India [9]. In a 2019 study, Yan Dong investigated groundwater-level variations in the Mid-Atlantic coastal plain of the United States. The research employed linear regression analysis to quantify long-term hydrological trends, supplemented by spatial hotspot analysis that identified statistically significant clusters of monitoring wells exhibiting either rising or declining water levels [10]. Precipitation recharge exerts a significant influence on groundwater dynamics. Li et al.'s study in the Shiyang River Basin in the arid zone showed that urbanization accelerated the rainfall-runoff process and shortened the residence time of the river (shortest in the middle reaches). Urban dam construction led to isotopic enrichment of river and groundwater, exacerbating evaporative losses and enhancing the hydraulic connection between the two. These isotope-based ecohydrological observations provide an important scientific basis for regional water resource management and urban planning [11]. Furthermore, intensive groundwater extraction has induced dramatic water-table fluctuations and triggered environmental geological issues, including seawater intrusion. Tran et al. employed the SEAWAT model (a variable-density groundwater flow and solute transport model) to demonstrate that groundwater abstraction and alterations in regional groundwater flow systems significantly influence water-level variations in the coastal aquifer of Vietnam's Mekong Delta [12]. Mao et al. applied a multi-isotope approach to investigate recharge sources in the Nantong region (southern Jiangsu Coastal Plain), demonstrating that local precipitation constitutes the primary recharge source for shallow groundwater. Their study revealed that declining groundwater levels have exacerbated seawater intrusion in the area [13]. Moreover, simulation studies have been conducted to assess groundwater dynamics influenced by natural factors (e.g., precipitation and

temperature). Jeihouni et al. evaluated the impacts of precipitation and temperature variations on groundwater levels in Iran's Shabestar Plain. Their projections indicate a regional decline in precipitation over the coming decades, which would lead to a sustained drop in average groundwater levels and the continued depletion of groundwater resources [14]. These findings underscore the necessity of incorporating extraction policies into water resource management frameworks. Boufekane et al. conducted groundwater modeling of the Jijel Plain aguifer in the southern Mediterranean region, revealing that water-table fluctuations and recharge patterns constitute critical factors controlling aquifer vulnerability to seawater intrusion [15]. Vespasiano et al. employed hydrogeochemical and isotopic analyses to investigate recharge processes in the shallow aquifer system of the Gioia Tauro Plain, one of southern Italy's most industrialized and agriculturally significant coastal regions. Their study demonstrated that local precipitation serves as the primary recharge source for groundwater in this aquifer system [16]. However, anthropogenic activities have induced more pronounced alterations in both groundwater table dynamics and hydrochemical environments. A case in point is the study by Bahir et al., which revealed that while the aquifer in Morocco's Essaouira Basin primarily receives recharge from Atlantic-origin precipitation, groundwater quality has been significantly compromised by domestic wastewater infiltration [17]. Peng et al. conducted a comprehensive study on groundwater dynamics in eastern China, revealing significant anthropogenic influences, including mine drainage, agricultural irrigation, and wastewater discharge on aquifer systems [18].

Consequently, groundwater dynamics in coastal plains exhibit complex behavior resulting from the combined effects of both natural and anthropogenic factors. Natural drivers include precipitation, evaporation, river recharge, lateral inflow, and tidal fluctuations, while human activities such as groundwater extraction, artificial recharge, irrigation practices, inter-basin water transfers, and ecological water supplementation significantly alter the natural regime [19, 20].

However, three key research gaps remain: (1) Limited quantification of how multiple drivers jointly control water-table changes; (2) Insufficient understanding of dynamic mechanisms in typical coastal cities; (3) Few validated strategies for balancing water use needs with resource protection— especially in rapidly developing areas.

To address these gaps, this study focuses on the Rizhao coastal plain groundwater system to investigate water-table fluctuation dynamics. The research employs three complementary approaches: (1) EOF analysis extracting spatiotemporal variation modes; (2) geospatial analysis quantifying groundwater depression center migration; (3) statistical correlation analysis identifying key factors. Findings provide scientific support for

sustainable management, extraction optimization, and ecological restoration in similar coastal settings.

### Study Area Overview

The study area is located in the coastal plain of Rizhao City, with an average elevation below 50 m. Characterized by a temperate monsoon climate, the region experiences four distinct seasons with high humidity and frequent typhoon events. The annual mean temperature is 12.7°C, with an average precipitation of 874 mm. The coastal plain has many rivers flowing into the sea. In the north are the Tianshui, Chaobai and Qinggang rivers. The central area has the Shadun, Gu, Futuan, and Chuanzi rivers. The south contains the Jufeng, Longwang, and Xiuzhen rivers. The mainland coastline of Rizhao City extends from the Baima River estuary in the north to the Xiuzhen River estuary in the south, with a total length of 226.35 km, including 32.45 km of natural coastline (14.33%), 167.45 km of artificial coastline (73.98%), and 26.45 km of other coastline (including estuaries and restored shoreline, accounting for 11.69%). The long and meandering coastline has complex effects on groundwater dynamics. The coastal districts of Donggang and Lanshan within the study area are densely populated coastal tourism cities and port cities. The anthropogenic influences on groundwater dynamics from nearby coastal agricultural irrigation zones and other human activities cannot be overlooked.

The groundwater primarily consists of Quaternary porous phreatic water, distributed across the midlower alluvial plains of river systems [21]. Additionally, bedrock fissure water is distributed in hilly and mountainous areas. The majority of the groundwater studied consists of porous phreatic water, which provides a prerequisite for selecting regional porous water monitoring wells. The dynamics of porous water are primarily influenced by atmospheric precipitation [22]. The intensive groundwater exploitation in the region has induced complex variations in both groundwater depth and aquatic environments [23]. The hydrogeological conditions of the study area are illustrated in Fig. 1.

#### **Materials and Methods**

### Data Acquisition

Groundwater depth data were collected on-site from 20 monitoring wells in the coastal plain of Rizhao between 2018 and 2020. The wells were distributed across the study area to capture spatial variability. The depth was aligned with the Quaternary porous phreatic aquifer to ensure consistency. Data were recorded monthly to analyze seasonal trends.

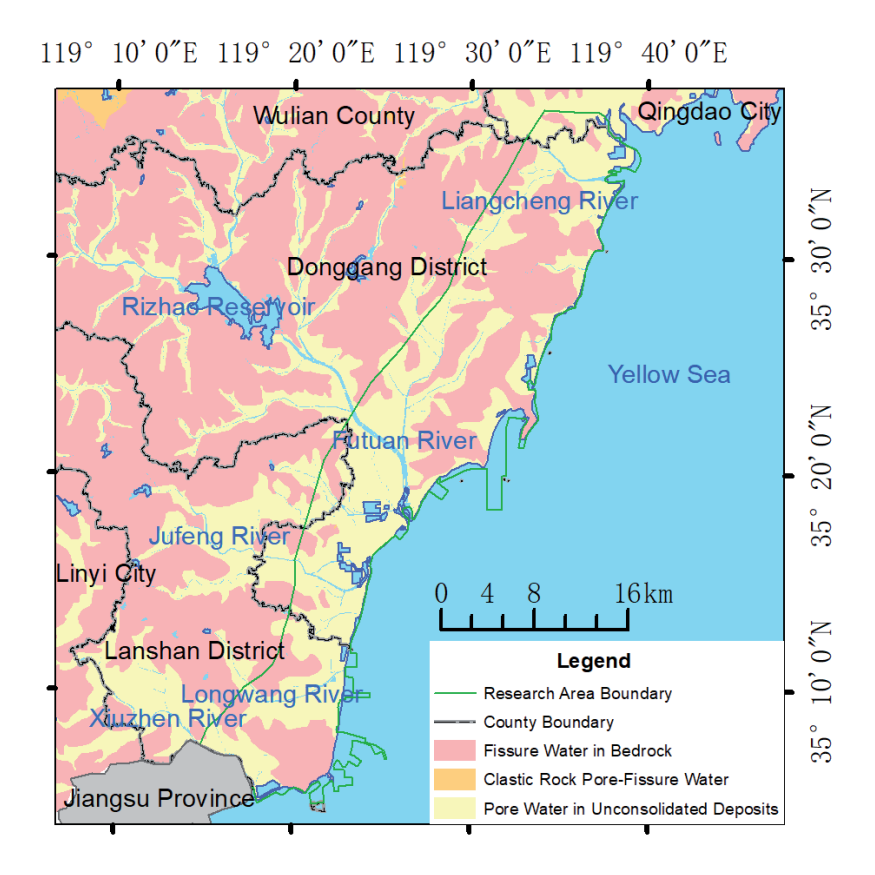


Fig. 1. Hydrogeological map.

### Empirical Orthogonal Function (EOF) Analysis

The Empirical Orthogonal Function (EOF) method was initially proposed by statistician Pearson in the early 20<sup>th</sup> century and was first applied to atmospheric science by Lorenz in 1950. The EOF method analyzes spatiotemporal datasets by decomposing an element field into a linear combination of spatial functions (independent of temporal variation) and temporal functions (dependent solely on time variation), thereby elucidating the spatiotemporal structure of the field. This approach has been extensively applied in geoscience research [24-26].

The EOF method constructs a spatiotemporal matrix from time-series data observed at different locations, then decomposes this matrix into the product of temporal and spatial matrices. By extracting the leading components of both spatial and temporal functions, it forms a new matrix that captures the majority of information from the original spatiotemporal field.

In this paper, the monthly groundwater depth data of 20 monitoring wells in 2018~2020 are calculated  $X = (x_{it})$  (i = 1, 2, ..., m, t = 1, 2, ... n). The m and n are the number of monitoring wells and the number of months, respectively.

Prior to decomposition, data preprocessing is essential: Temporal centering (removing station-wise means) and Optional standardization.

$$\bar{x}_i = \frac{1}{n} \sum_{t=1}^n x_{it} \quad (j = 1, 2, ..., m)$$
 (1)

$$\tilde{x}_{it} = x_{it} - \bar{x}_i \tag{2}$$

$$\sigma_i = \sqrt{\frac{1}{n-1}} \sum_{t=1}^{n} (x_{it} - \bar{x}_i)^2$$
 (3)

$$\hat{x}_{it} = \frac{\tilde{x}_{it}}{\sigma_i} \tag{4}$$

where  $\bar{\mathcal{X}}_i$  represents the average water level at all moments in well i;  $\tilde{\mathcal{X}}_{it}$  centered data (i.e., outliers that deviate from the mean);  $\sigma_i$  the standard deviation of the time series of water depths in well i; and  $\hat{\mathcal{X}}_{it}$  the relative fluctuation intensity: how many standard deviations from the mean is the current depth of burial.

The matrix X can be decomposed into a spatial function matrix A and a temporal matrix B.

$$X = AB \tag{5}$$

$$X_{it} = \sum_{k=1}^{m} a_{it} b_{it} \tag{6}$$

$$\mathbf{A} = (a_1, a_2, \cdots, a_m) = \begin{bmatrix} a_{11} & \cdots & a_m \\ \vdots & \ddots & \vdots \\ a_{1m} & \cdots & a_{mm} \end{bmatrix}$$
(7)

$$\mathbf{B} = \begin{bmatrix} b_{11} & \cdots & b_{1n} \\ \vdots & \ddots & \vdots \\ b_{m1} & \cdots & b_{mn} \end{bmatrix} \tag{8}$$

 $a_j = (a_{j1}, a_{j2}, ..., a_{jm})^T$ . This corresponds to the j-th empirical orthogonal mode (EOF mode), which is a spatial-dependent function exclusively determined by geographic coordinates.

# Spatial Analysis

Spatial interpolation was performed using ArcGIS to map the spatial distribution of different characteristic vectors. The mean center analysis was conducted by weighting based on groundwater depth values to calculate the mean center position of the groundwater table.

$$\bar{X}_{w} = \frac{\sum_{i=1}^{n} w_{i} x_{i}}{\sum_{i=1}^{n} w_{i}}$$
(9)

$$\bar{Y}_{w} = \frac{\sum_{i=1}^{n} w_{i} y_{i}}{\sum_{i=1}^{n} w_{i}}$$
(10)

Here, i = 1, 2, 3, ..., n represents the number of monitoring wells,  $\overline{X}_w$  is the x-coordinate of the mean center of groundwater depth,  $\overline{Y}_w$  is the y-coordinate of the mean center, and  $w_i$  is the weight at location i, calculated based on groundwater level depth.

## Correlation Analysis

Correlation analysis between groundwater depth eigenvectors and precipitation was conducted using SPSS, with significance testing performed. The Pearson correlation coefficient (r) is calculated as follows:

$$\rho_{xy} = \frac{cov(x,y)}{\sigma(x)\sigma(y)} = \frac{E[(x - \mu_x)(y - \mu_y)]}{\sigma(x)\sigma(y)}$$
(11)

Here, x is the monthly precipitation and y is the monthly groundwater depth eigenvector.

### Data

The data used in this study mainly include: (1) monthly average groundwater depth data from 20 national groundwater monitoring wells in the Rizhao coastal plain during 2018-2020; (2) monthly precipitation data calculated from daily precipitation records at the national meteorological station (Rizhao Station) from 2018 to 2020; (3) annual groundwater withdrawal data of Rizhao City for 2018-2020.

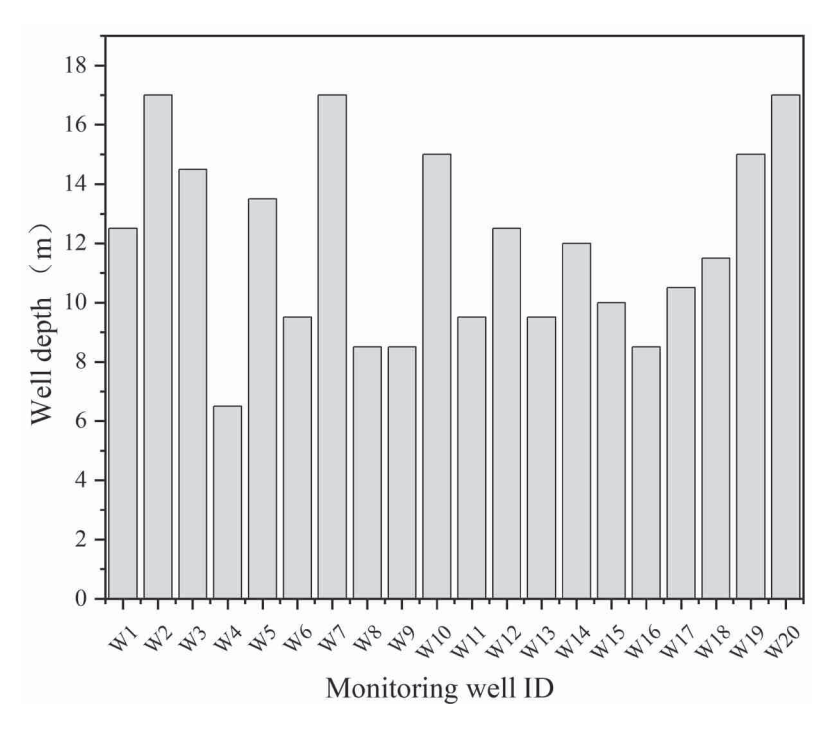


Fig. 2. Depth map of different observation Wells.

The 20 monitoring wells are relatively uniformly distributed in the study area. Wells W10, W13, W14, and W17 are located on the right bank of the Tianshui River and the left bank of the Chaobai River in the estuary area of the northern boundary. Wells W11 and W16 are situated on the left bank of the Shadun River in the coastal region. Wells W1, W2, W12, and W20 are distributed in the estuarine area on both banks of the Futuan River in the central zone. Wells W3, W4, and W5 are located in the coastal area on both banks of the Chuanzi River. W15 is situated on the right bank of the Jufeng River. Wells W8 and W19 are positioned on both banks of the Longwang River. Wells W18 is located in the plain area between the Longwang River and the Jufeng River. Wells W6, W7, and W9 are situated in the left bank area of the Xiuzhen River at the southern boundary. The meteorological station S1 is located within the premises of the Donggang District Meteorological Bureau in Rizhao City.

### Results

# Temporal Variation Characteristics of Groundwater Depth

As shown in Fig. 4, the groundwater level depth exhibits both annual and monthly fluctuations. In 2018, the maximum average groundwater depth (3.52 m) in the study area occurred in February, while the minimum (2.47 m) was observed in September. In 2019, the months of extreme values shifted, with the maximum depth (3.92 m) recorded in December and the minimum (3.24 m) in August. In 2020, the maximum average groundwater

depth (4.46 m) in the study area occurred in April, while the minimum (2.38 m) was observed in August. The seasonal variation characteristics over the three-year period consistently showed smaller interquartile ranges of groundwater depth in summer and autumn compared to winter and spring, with groundwater depths being regionally more clustered during spring and summer seasons.

The mean center results of groundwater depth are shown in Fig. 5. Fig. 5a) displays the annual variation of average groundwater depth, revealing that in 2018, the mean center was distributed in a northeast-southwest orientation, located northwest of the study area's center. In 2019, the mean center shifted southeastward, with an overall smaller displacement distance compared to 2018. In 2020, the mean center of groundwater depth migrated southwestward, with two distinct clusters emerging: a northeastern cluster overlapping with the 2018 and 2019 clusters, and a newly formed southwestern cluster also exhibiting a northeast-southwest orientation. The linear trend lines fitted to the mean centers of groundwater depth for different years are presented in Table 1.

The temporal coefficient curves obtained from EOF decomposition are shown in Fig. 6. Fig. 6 reveals significant variations in the temporal coefficients across different principal component modes.

The temporal coefficient of the first eigenvector (PC1) reaches its peak during March-April and its trough in August each year. The 2019 trough was nearly five times greater than those in 2018 and 2020. After reaching the minimum value in August, it rebounds sharply, while after peaking in March-April of 2018 and 2019, it declines gradually, contrasting with the abrupt decrease observed in 2020. The temporal coefficient

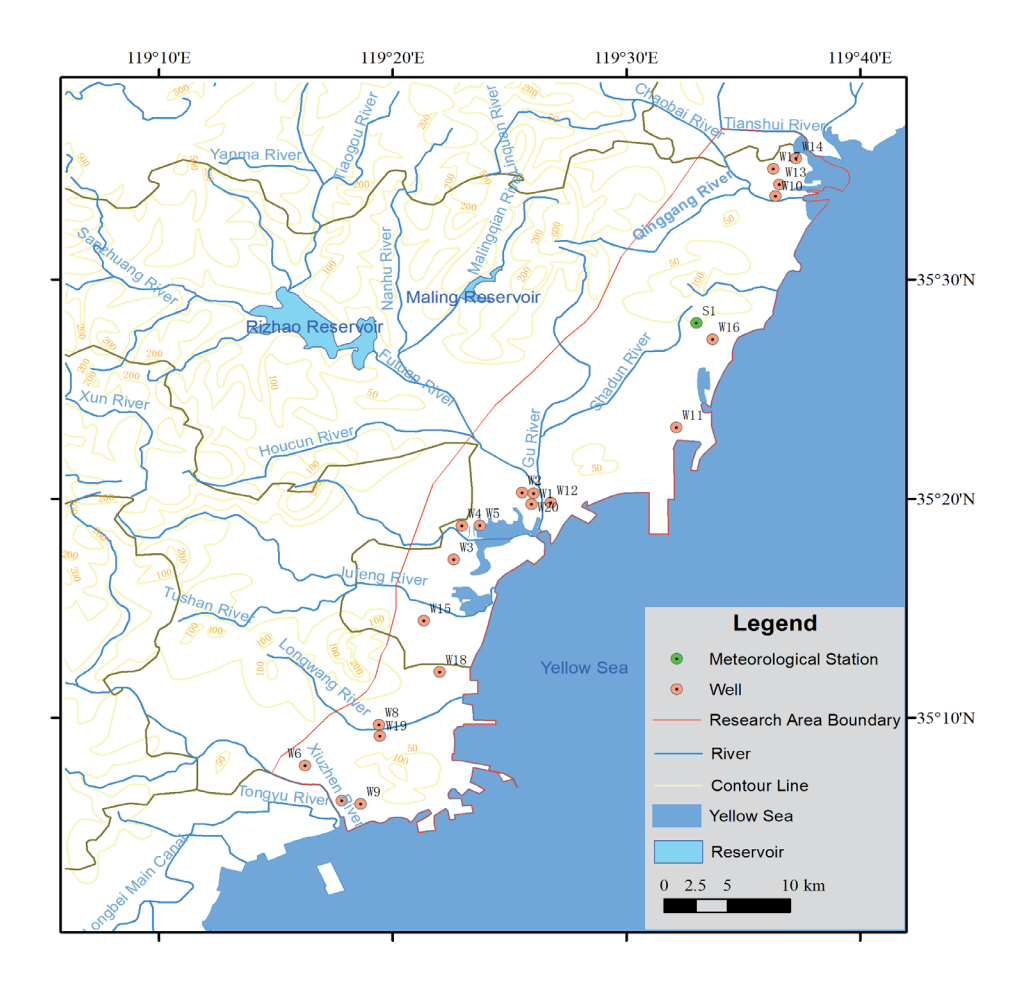


Fig. 3. Map of monitoring sites.

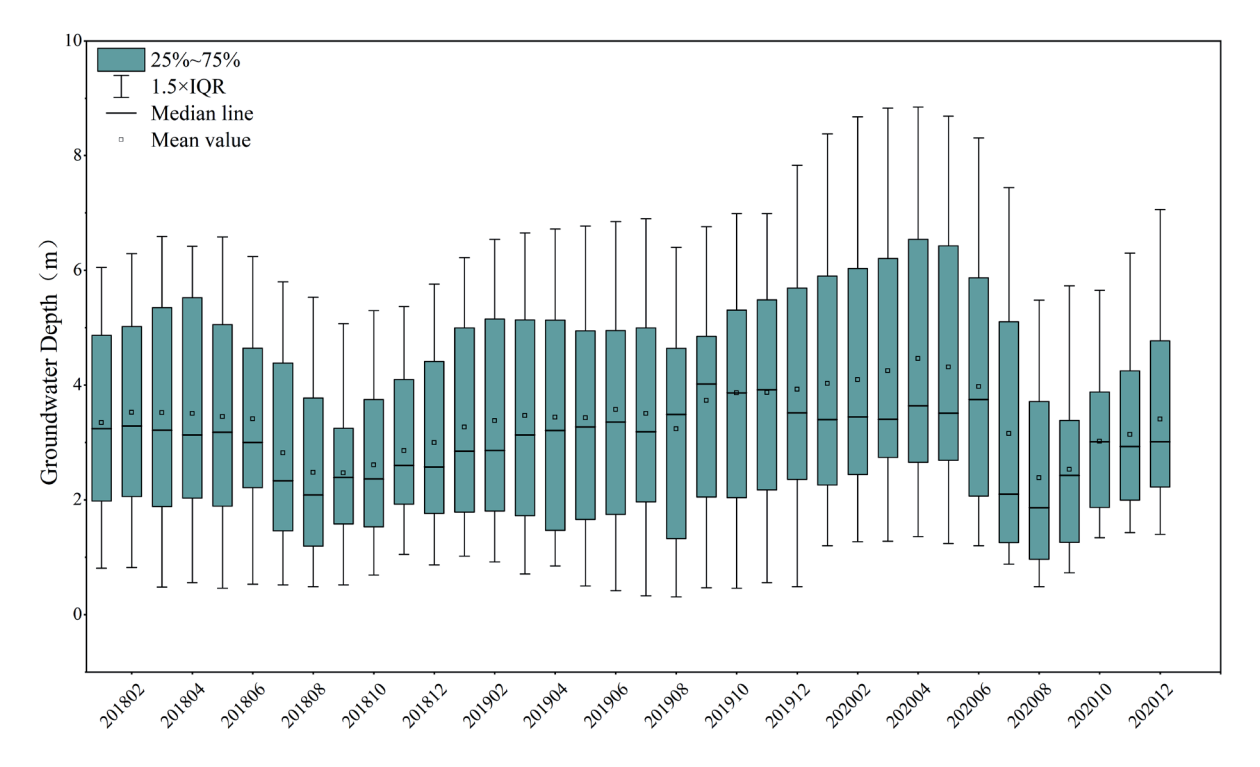


Fig. 4. Monthly statistics of groundwater depth in different years.

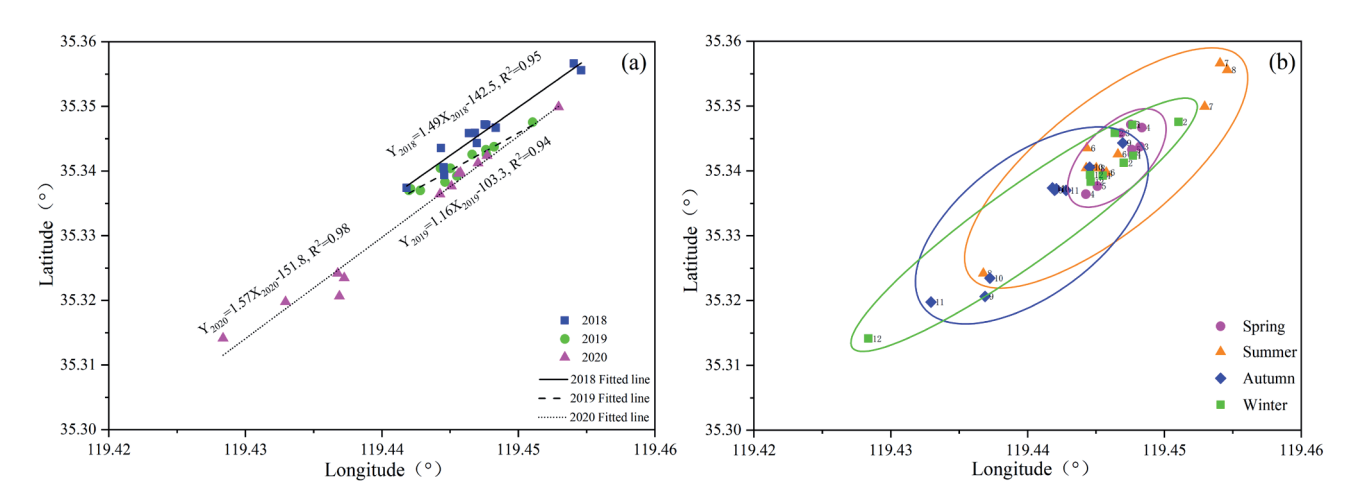


Fig. 5. Annual and seasonal variations of mean central groundwater depth. a) Annual change in depth to groundwater, b) Seasonal variations in depth to groundwater.

Table 1. Linear fitting table of the average center of groundwater depth in different years.

Year	Fitting equation	Correlation coefficient (R <sup>2</sup> )	Residual sum of squares (RSS)
2018	$Y_{2018} = 1.49X_{2018} - 142.5$	0.95	1.8×10 <sup>-5</sup>
2019	$Y_{2019} = 1.16X_{2019} - 103.3$	0.94	7.0×10 <sup>-6</sup>
2020	$Y_{2020} = 1.57X_{2020} - 151.8$	0.98	3.3×10 <sup>-5</sup>

of the second eigenvector (PC2) shows an overall downward trend over the three-year period, with slow increases after August 2018 and August 2020, but begins to fluctuate and decline monthly after August 2019. The minimum value (4.80) occurred in September 2020, while the maximum (2.90) appeared in June 2018.

For the third eigenvector (PC3), the temporal coefficient showed monthly fluctuations increasing to a peak (2.80) before September 2019, followed by oscillating declines to a trough (-1.20) in March 2020. Subsequently, a peak (0.84) emerged in August 2020. The temporal coefficient of the fourth eigenvector (PC4) consistently displayed

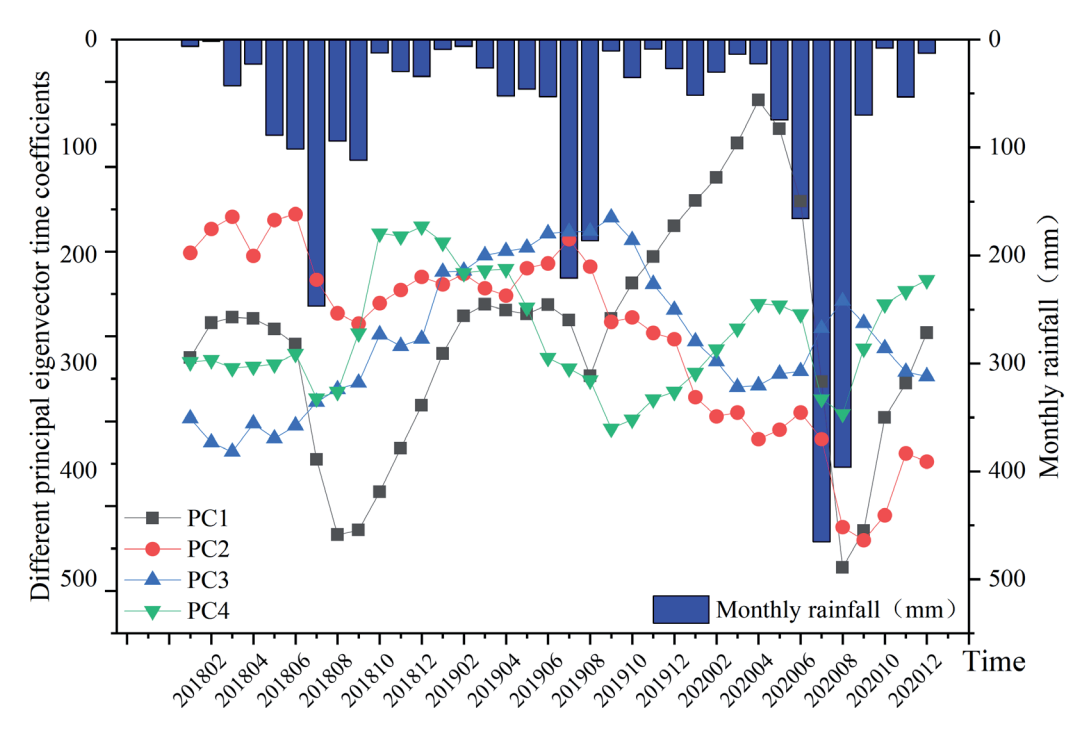


Fig. 6. Time coefficients of different feature vectors and monthly precipitation graphs.

August troughs during 2018-2020 (-1.46, -2.17, and -1.83, respectively), with winter-spring peaks occurring in December 2018 (2.60) and April 2020 (0.77).

Fig. 6 shows the temporal heterogeneity of precipitation in the bar chart. The annual precipitation in 2018 was 793.3 mm, while that in 2019 was 0.86 times that of 2018. In contrast, 2020 experienced more heavy rainfall events, with precipitation reaching twice the 2018 level. On average, summer rainfall accounted for 66.4% of the annual total, followed by autumn (14.5%), spring (12.7%), and winter (6.4%).

# Spatial Distribution Characteristics of Groundwater Depth

Using the EOF method, the spatiotemporal field composed of groundwater depth was decomposed, and the characteristic results of the correlation matrix are shown in Table 2. The ratio represents the variance contribution corresponding to the eigenvalue, while the cumulative value indicates the accumulated variance of the preceding principal components. As shown in Table 2, the eigenvalues of the first four factors are all greater than 1, and the cumulative contribution of the first four principal components reaches 83.3%. Therefore, the first four principal components can effectively capture the majority of the key information from the original spatiotemporal field of groundwater depth. The variance contribution of the first principal component (PC1) is 36.7%, followed by the second principal component (PC2) at 24.2%, the third principal component (PC3) at 13.4%, and the fourth principal component (PC4) at 8.9%.

The first four principal eigenvectors were projected onto the corresponding monitoring well locations on the map, and isoline analysis was performed in ArcGIS to obtain spatial distribution maps of groundwater depth for different principal eigenvectors, as shown in Fig. 7.

The spatial distribution maps of different eigenvectors after EOF decomposition focus on the first four eigenvectors. All values of the first eigenvector are positive, ranging from 0.1 to 0.35. As shown in Fig. 7a), the first eigenvector exhibits three extreme value regions within the study area: a maximum value zone (PC1>0.3) located at the confluence of the Futuan River and Gu River, including monitoring wells W1 and W2; and two minimum value zones (PC1<0.1) one situated along the left bank of the lower reaches of Chuanzi River containing monitoring well W5, and another located on the right bank of Tianshui River at the northern boundary including monitoring well

W14. The remaining areas in the study region show alternating distributions of high and low value zones between landward and seaward sides.

The second eigenvector exhibits three minimum value zones (PC2<-0.3): the first extreme zone appears near W14 on the right bank of the Xiuzhen River, the second minimum zone is distributed near W16 in the coastal area of the upper reaches of the Shadun River, and the third minimum zone is located near W8 in the Longwang River basin. Additionally, the second eigenvector contains one maximum value zone (PC2>0.3), which is distributed in the area near W6 on the right bank of the Xiuhuazhen River, as in Fig. 7b).

Fig. 7c) shows that the third eigenvector exhibits three maximum value zones (PC3>0.3): the first maximum zone covers a broad area near W11 in the Rizhao urban district, the second extreme zone is located near W15, and the third extreme zone is situated near W9 in the southern region. The third eigenvector also contains one minimum value zone (PC3<-0.4) located near W5 on the left bank of the Chuanzi River.

The fourth eigenvector shows three maximum value zones (PC4>0.3): the first maximum zone is situated near W14 on the right bank of the Tianshui River, the second maximum zone is located near W11 in the Rizhao urban district, and the third maximum zone is found near W7 on the left bank of the Xiuzhen River. Additionally, the fourth eigenvector contains one minimum value zone (PC4<-0.4) located near W12 on the left bank of the main channel formed by the confluence of the Futuan River and Gu River, see Fig. 7c).

The first four principal feature vectors of groundwater depth derived from EOF decomposition reveal distinct spatial patterns: PC1 (all positive values: 0.1-0.35) exhibits three extreme-value zones - a maximum zone (>0.3) at the Futuan-Gu River confluence (W1, W2), and two minimum zones (<0.1) at the lower Chuanzi River's left bank (W5) and Tianshui River's right bank (W14), with remaining areas showing land-sea alternation of high/low values; PC2 forms three minimum-value zones (<-0.3) along the Xiuzhen River (W14), Shadun River coast (W16), and Longwang River (W8), while displaying a maximum zone (>0.3) on the Xiuhuazhen River's right bank (W6); PC3 contains three maximumvalue zones (>0.3) in Rizhao urban area (W11), near W15, and southern region (W9), whereas the Chuanzi River's left bank (W5) constitutes a minimum zone (<-0.4); PC4 displays three maximum-value zones (>0.3) at Tianshui River (W14), Rizhao urban area (W11), and Xiuzhen River's left bank (W7), with a minimum

Table 2. Correlation matrix feature analysis results.

Tuoto 2. Confedenti matrix reactive anarysis results.					
Item	PC1	PC2	PC3	PC4	
Eigenvalue	7.3451	4.8414	2.684	1.7898	
Ratio	0.367	0.242	0.134	0.089	
Cumulative	0.367	0.609	0.744	0.833	

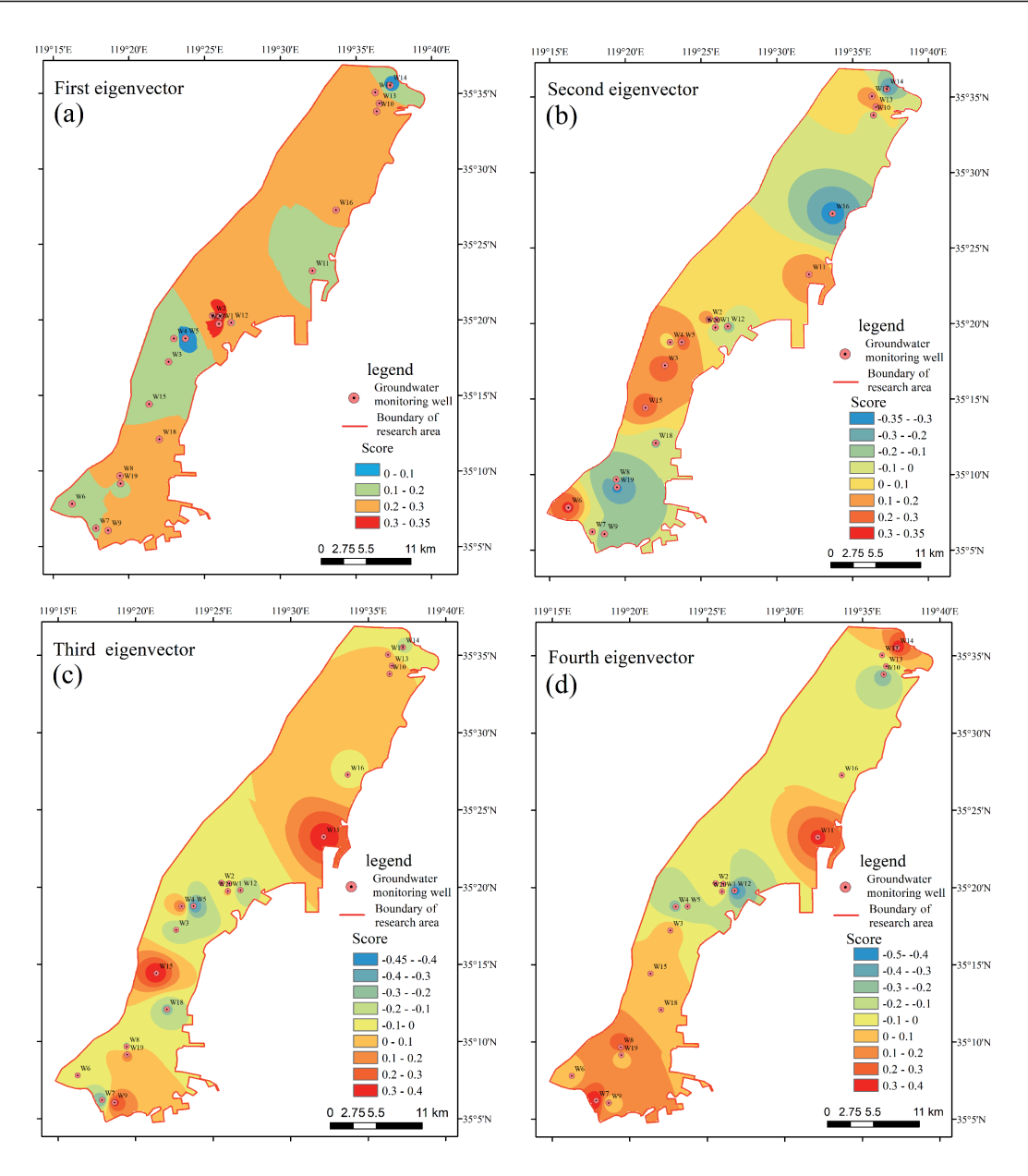


Fig. 7. EOF decomposition of different feature vector space distribution. a) First eigenvector, b) Second eigenvector, c) Third eigenvector, d) Fourth eigenvector.

zone (<-0.4) on the Futuan-Gu River mainstem's left bank (W12). These patterns demonstrate PC1's dominance in global spatial consistency, while higher-order vectors (PC2-PC4) reveal local heterogeneity through extreme-value distributions, their spatial differentiation being intrinsically linked to river networks and monitoring sites.

# Discussion

Impact of Precipitation on Principal Eigenvectors of Groundwater Depth

Fig. 6 demonstrates that summer and autumn precipitation collectively account for 80.9% of the

annual total. The principal eigenvectors of groundwater depth (PC1 and PC4) exhibit synchronous fluctuation patterns with seasonal precipitation variations. Notably, when precipitation reaches its peak, PC1 and PC4 display a 1-2 months lag before attaining their trough values. This temporal delay primarily results from the time required for precipitation infiltration and runoff generation/concentration processes, which consequently leads to the hysteresis of groundwater level responses relative to precipitation variations [27-29]. PC2 and PC3 exhibit inverse trends in response to seasonal precipitation variations. Specifically, PC3 reaches its peak value with a 2-month lag following the month of maximum rainfall, while PC2 attains its trough value with a 1-2 months delay after the peak precipitation period. To quantitatively examine the relationships

Table 3. Table of the relationship between time coefficients of
different characteristic components of groundwater depth and
precipitation.

Time Coefficient	Statistic	Precipitation
PC1	Correlation	334*
rcı	Significance (Two-tailed)	0.046
PC2	Correlation	-0.222
PC2	Significance (Two-tailed)	0.192
PC3	Correlation	0.07
PC3	Significance (Two-tailed)	0.685
PC4	Correlation	406*
FC4	Significance (Two-tailed)	0.014

<sup>\*.</sup> Correlation is significant at the 0.05 level (2-tailed).

between precipitation and these principal eigenvectors, correlation analysis was conducted, with the results presented in Table 3.

As indicated by the correlation analysis between monthly precipitation and principal eigenvectors in Table 3, PC1 and PC4 exhibit negative correlations with monthly precipitation (r = -0.334 and -0.406, respectively), both statistically significant at the 0.05 level (two-tailed p-values: 0.046 and 0.014). Combined with the spatial analysis results from Fig. 7, this demonstrates that PC1 and PC4 represent precipitation-influenced eigenvectors that significantly contribute to groundwater depth dynamics. Consequently, the cumulative contribution of PC1 and PC4 (45.6%) quantitatively reflects precipitation's influence on regional groundwater systems. The non-significant correlations of PC2 and PC3 (combined contribution:

54.4%) likely result from the combined effects of other natural factors and anthropogenic activities.

# Impacts of Socioeconomic Development on Groundwater Resources

The Donggang and Lanshan districts in the study area primarily utilize shallow phreatic water as their water supply source. As shown in Fig. 8, the groundwater supply in Lanshan District, Rizhao City, was relatively limited - maintaining 11.25 million m³ in both 2018 and 2019, before increasing sharply to 38.45 million m³ in 2020 (a 3.42-fold increase). In contrast, Donggang District's groundwater supply volumes were 39.65 million m³ (2018) and 38.45 million m³ (2019), with a modest increase to 41.05 million m³ in 2020.

As shown in Fig. 5, the average centroid of groundwater depth shifted southwestward in 2020, forming a new concentrated area. Combined with Fig. 8, this phenomenon can be attributed to increased groundwater extraction for water supply in the Lanshan District during 2020 compared to 2018-2019 levels, which resulted in greater groundwater depth and caused the overall southwestward migration of the study area. This demonstrates that the average centroid of groundwater depth is associated with anthropogenic groundwater extraction. To maintain the dynamic equilibrium of regional groundwater levels and protect aquifers from seawater intrusion [29-31], it is necessary to implement both localized key controls and regional coordinated management. This involves rationally planning and dynamically adjusting the spatial distribution of socio-economic activities, as well as modifying water supply patterns and total volumes. Through policy guidance, sustainable

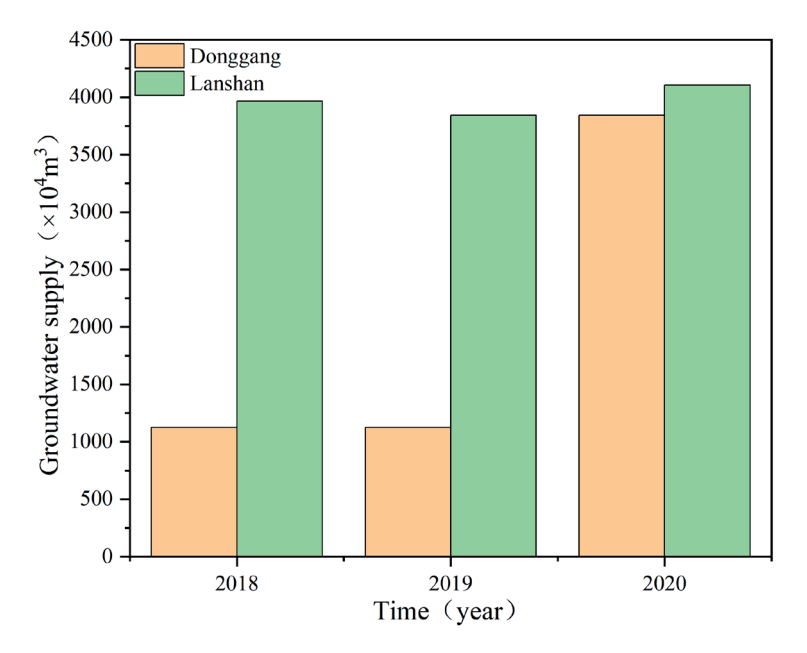


Fig. 8. Column chart of groundwater supply in Rizhao in different years.

<sup>\*\*.</sup> Correlation is significant at the 0.01 level (2-tailed).

development and utilization of groundwater resources can be achieved.

**Conclusions** 

Utilizing groundwater depth monitoring data from 20 observation wells in the Rizhao coastal plain (2018-2020), this study employed empirical orthogonal function (EOF) decomposition alongside spatial and correlation analyses to investigate groundwater dynamics and their driving factors. Key findings include:

- (1) Groundwater depth centroid dynamics: Exhibiting both interannual and seasonal variations, centroid distributions demonstrated smaller variability in summer/autumn than winter/spring, with greater spatial clustering during spring/summer. The centroid displayed a NE-SW orientation northwest of the study area's center in 2018, shifted southeastward in 2019, and migrated southwestward in 2020 the latter forming a new concentration zone with similar NE-SW alignment.
- (2) EOF-based spatial heterogeneity: Variance contributions were PC1 (36.7%), PC2 (24.2%), PC3 (13.4%), and PC4 (8.9%), cumulatively explaining 83.2% of variability. Maximum-value zones of PC1 and PC2 clustered near riverbanks, whereas PC3 and PC4 maxima concentrated around urban areas.
- (3) Lagged response to precipitation: Groundwater depth exhibited 1-2 months lags behind precipitation events. Precipitation accounted for 45.6% of groundwater dynamics, with other natural/anthropogenic factors collectively contributing 54.4% as quantified by variance decomposition.
- (4) Based on spatial groundwater heterogeneity (PC1-PC4 dominant patterns) and centroid migration dynamics revealed through EOF decomposition, combined with the 1-2 months precipitation lag response and dominant anthropogenic drivers (54.4%), we propose differentiated control zones with operational measures:

River-Sensitive Zone (PC1/2 high-value): Strict well density control, riverine no-extraction buffers, water-efficient irrigation promotion.

Urban Pressure Zone (PC3/4 clusters): Extraction quotas, mandatory rainwater recharge infrastructure, enhanced reclaimed water utilization.

Agri-Regulation Zone (centroid hotspots): Lowwater-demand cultivars implementation, precision irrigation allocation systems.

Transition Zones (low/mixed PC): Groundwater equilibrium maintenance, localized over-extraction, and contamination risk mitigation.

### **Author Contributions**

Conceptualization, Yuan Jie.; methodology, Zhao Xiaoxin; writing – review and editing, Yao Dongxu;

visualization, Wei Tongzheng; formal analysis, Lv Youcheng.

### **Funding**

This research was funded by Basic Survey and Monitoring of Water Resources in the Rizhao Reservoir, grant number [DZG202402].

### Data availability

The datasets used and/or analyzed during the current study are available from the corresponding author on reasonable request.

### Acknowledgements

We would like to express our sincere thanks to the editors and reviewers for their very helpful comments on the paper.

### **Conflict of interest**

The authors declare no competing interests.

#### References

- LAPWORTH D., BOVING T., BRAUNS B., DOTTRIDGE J., HYNDS P., KEBEDE S., KREAMER D., MISSTEAR B., MUKHERJEE A., RE V., SORENSEN J., VARGAS C.R. Groundwater quality: global challenges, emerging threats and novel approaches. Hydrogeology Journal. 31 (1), 15, 2023.
- EDET A., ABDELAZIZ R., MERKEL B., OKEREKE C., NGANJE T. Numerical Groundwater Flow Modeling of the Coastal Plain Sand Aquifer, Akwa Ibom State, SE Nigeria. Journal of Water Resource and Protection. 6 (4), 193, 2014.
- 3. ZAMRSKY D., ESSINK G.H.P.O., SUTANUDJAJA E.H., VAN BEEK L.P.H., BIERKENS M.F.P. Offshore fresh groundwater in coastal unconsolidated sediment systems as a potential fresh water source in the 21<sup>st</sup> century. Environmental Research Letters. 17 (1), 2022.
- COSTALL A.R., HARRIS B.D., TEO B., SCHAA R., WAGNER F.M., PIGOIS J.P. Groundwater Throughflow and Seawater Intrusion in High Quality Coastal Aquifers. Scientific Reports. 10 (1), 2020.
- ADHIKARI R.K., YILMAZ A.G., MAINALI B., DYSON P., IMTEAZ M.A. Methods of Groundwater Recharge Estimation under Climate Change: A Review. Sustainability. 14 (23), 2022.
- KETABCHI H., MAHMOODZADEH D., VALIPOUR E., SAADI T. Uncertainty-based analysis of water balance components: a semi-arid groundwater-dependent and data-scarce area, Iran. Environment Development and Sustainability. 26 (12), 31511, 2024.

 FAN X., MIN T., DAI X. The Spatio-Temporal Dynamic Patterns of Shallow Groundwater Level and Salinity: The Yellow River Delta, China. Water. 15 (7), 2023

- 8. CUI Z., CHEN G., CHEN S., YU H., CHEN K., RAN B., FU T., LYU W., WANG Y., JIANG X., ZHONG X. Groundwater salinization under the influence of paleo sealevel fluctuation: a case study in southern Laizhou Bay, China. Frontiers in Marine Science. 10, 2024.
- RAO N.S., DINAKAR A., SUN L. Estimation of groundwater pollution levels and specific ionic sources in the groundwater, using a comprehensive approach of geochemical ratios, pollution index of groundwater, unmix model and land use/land cover – A case study. Journal of Contaminant Hydrology. 248 (2), 103990, 2022.
- DONG Y., JIANG C., SURI M.R., PEE D., MENG L., GOLDSTEIN R.E.R. Groundwater level changes with a focus on agricultural areas in the Mid-Atlantic region of the United States, 2002-2016. Environmental Research. 171, 193, 2019.
- 11. LI R., ZHU G.F., LU S.Y., SANG L.Y., MENG G.J., CHEN L.H., JIAO Y.Y., WANG Q.Q. Effects of urbanization on the water cycle in the Shiyang River basin: based on a stable isotope method. Hydrology and Earth System Sciences. 27 (24), 4437, 2023.
- 12. DANG AN T., TSUJIMURA M., PHAM H.V., NGUYEN T.V., LOC HUU H., PHU LE V., KHAI QUANG H., THANH DUC D., DOAN VAN B., QUANG-VAN D. Intensified salinity intrusion in coastal aquifers due to groundwater overextraction: a case study in the Mekong Delta, Vietnam. Environmental Science and Pollution Research. 29 (6), 8996, 2022.
- 13. MAO C., TAN H., SONG Y., RAO W. Evolution of groundwater chemistry in coastal aquifers of the Jiangsu, east China: Insights from a multi-isotope (δ<sup>2</sup>H, δ180, <sup>87</sup>Sr/<sup>86</sup>Sr, and δ<sup>11</sup>B) approach. Journal of Contaminant Hydrology. **235**, **2020**.
- 14. JEIHOUNI E., MOHAMMADI M., ESLAMIAN S., ZAREIAN M.J. Potential impacts of climate change on groundwater level through hybrid soft-computing methods: a case study-Shabestar Plain, Iran. Environmental Monitoring and Assessment. 191 (10), 2019.
- BOUFEKANE A., MAIZI D., MADENE E., BUSICO G., ZGHIBI A. Hybridization of GALDIT method to assess actual and future coastal vulnerability to seawater intrusion. Journal of Environmental Management. 318, 2022.
- 16. VESPASIANO G., CIANFLONE G., MARINI L., DE ROSA R., POLEMIO M., WALRAEVENS K., VASELLI O., PIZZINO L., CINTI D., CAPECCHIACCI F., BARCA D., DOMINICI R., APOLLARO C. Hydrogeochemical and isotopic characterization of the Gioia Tauro coastal Plain (Calabria-southern Italy): A multidisciplinary approach for a focused management of vulnerable strategic systems. Science of the Total Environment. 862, 2023.
- 17. BAHIR M., OUAZAR D., OUHAMDOUCH S. Characterization of mechanisms and processes controlling groundwater salinization in coastal semi-arid area using hydrochemical and isotopic investigations (Essaouira basin, Morocco). Environmental Science and Pollution Research. 25 (25), 24992, 2018.
- PENG C., HE J.-T., WANG M.-L., ZHANG Z.-G., WANG L. Identifying and assessing human activity impacts on

- groundwater quality through hydrogeochemical anomalies and NO<sub>3</sub>, NH<sub>4</sub>, and COD contamination: a case study of the Liujiang River Basin, Hebei Province, PR China. Environmental Science and Pollution Research. **25** (4), 3539, **2018**.
- 19. JI Z., CUI Y., ZHANG S., CHAO W., SHAO J. Evaluation of the Impact of Ecological Water Supplement on Groundwater Restoration Based on Numerical Simulation: A Case Study in the Section of Yongding River, Beijing Plain. Water. 13 (21), 2021.
- MOHAN C., GLEESON T., FORSTNER T., FAMIGLIETTI J.S.S., DE GRAAF I. Quantifying Groundwater's Contribution to Regional Environmental-Flows in Diverse Hydrologic Landscapes. Water Resources Research. 59 (6), 2023.
- 21. GAO Z., ZHANG H., SUN M., XU H., YAO D.J.G.W. The chemical characteristics and causes of shallow groundwater in the Rizhao coastal area of Shandong province are discussed. Ground Water. 39, 1, 2017.
- YANG P., YUAN J., QING P.J.A.G.S. Dynamic characteristics and evolution law of groundwater in Rizhao City, Shandong. Acta Geologica Sinica. 93 (S1), 100, 2019.
- MANCUSO M., SANTUCCI L., CAROL E. Effects of intensive aquifers exploitation on groundwater salinity in coastal wetlands. Hydrological Processes. 34 (11), 2313, 2020.
- 24. CHEN Z. Spatial and temporal distribution characteristics of precipitation in different seasons in Heilongjiang Province from 1954 to 2013. EDP Sciences, 2022.
- 25. ÇELIK A., ALTUNKAYNAK A.J. Optimization of Precipitation Monitoring Network via Robust Empirical Orthogonal Function Analysis with QR Column Pivoting. Journal of Hydrologic Engineering. 29 (3), 04024007, 2024.
- 26. SUN M., KIM G., XU X., WANG Y. Investigation of South Korea precipitation variation using empirical orthogonal function (EOF) and cyclostationary EOF. IOP Publishing, 2021.
- JI-HUI F., QIAO L., YAN Z., GEN-WEI C., XIANG-DE F., WEN-MING L.J.W.U.J.O.N.S. Dynamic variations and influencing factors of groundwater levels in Lhasa city. Wuhan University Journal of Natural Sciences. 10, 665, 2005.
- 28. YIN X., SHU L., WANG Z., LU C., LIU B.J.J.O.H. Time-frequency analysis of groundwater depth variation based on the ICA-WTC composite method. Journal of Hydrology. **617**, 128914, **2023**.
- 29. QU J., TIAN R., REN K., JIANG J., ZHOU J.J.A.G. Response of the shallow groundwater level to the changing environment in Zhongmu County, China. Acta Geophysica. 72 (5), 3427, 2024.
- XINQIANG D., KAIYANG C., XIANGQIN L.J.W.S. Characteristics and causes of groundwater dynamic changes in Naoli River Plain, Northeast China. Water Supply. 20 (7), 2603, 2020.
- 31. WANG W., TIAN H., YANG G., LIU B., PAN Y., DING G., XU X., DAN Y., CUI M., GAO Y.J. Dynamic variation of groundwater level and its influencing factors in typical oasis irrigated areas in Northwest China. Open Geosciences. 15 (1), 20220493, 2023.